



HAL
open science

Quantifying phonon and polariton heat conduction along polar dielectric nanofilms

Yangyu Guo, Jose Ordonez-Miranda, Yunhui Wu, Sebastian Volz

► **To cite this version:**

Yangyu Guo, Jose Ordonez-Miranda, Yunhui Wu, Sebastian Volz. Quantifying phonon and polariton heat conduction along polar dielectric nanofilms. *Journal of Applied Physics*, 2024, 136 (4), pp.044303. 10.1063/5.0214699 . hal-04662717

HAL Id: hal-04662717

<https://hal.science/hal-04662717>

Submitted on 26 Jul 2024

HAL is a multi-disciplinary open access archive for the deposit and dissemination of scientific research documents, whether they are published or not. The documents may come from teaching and research institutions in France or abroad, or from public or private research centers.

L'archive ouverte pluridisciplinaire **HAL**, est destinée au dépôt et à la diffusion de documents scientifiques de niveau recherche, publiés ou non, émanant des établissements d'enseignement et de recherche français ou étrangers, des laboratoires publics ou privés.

Quantifying phonon and polariton heat conduction along polar dielectric nanofilms

Yangyu Guo ^{1*}, Jose Ordonez-Miranda ^{2,3}, Yunhui Wu ² and Sebastian Volz ^{2,3†}

¹ *School of Energy Science and Engineering, Harbin Institute of Technology, Harbin 150001, China*

² *Institute of Industrial Science, The University of Tokyo, Tokyo 153-8505, Japan*

³ *LIMMS, CNRS-IIS IRL 2820, The University of Tokyo, Tokyo 153-8505, Japan*

(Dated: June 25, 2024)

Abstract

The decisive experimental evidence of enhanced heat conduction driven by surface phonon polaritons (SPhPs) has been recently demonstrated along polar nanofilms. However, a proper quantitative interpretation remains to be fully established. In this work, we provide a consistent theoretical explanation of the measured thermal conductivities of polar nanofilms, based on a coupled Boltzmann transport equation and heat diffusion equation for describing the dynamics of SPhPs and phonons, respectively. This formalism enables to separately quantify the SPhP and phonon contributions to the in-plane heat transport and shows the overestimation of the SPhP thermal conductivity predicted by previous empirical model for the predominant boundary scattering. This study thus promotes the understanding of the observed thermal conductivity enhancement driven by SPhPs, as a novel heat conduction channel for heat dissipation applications in nanoelectronics and optoelectronics.

* yyguo@hit.edu.cn

† volz@iis.u-tokyo.ac.jp

1. Introduction

With the miniaturization of the micro- and nano-electronics, heat dissipation becomes a critical bottleneck due to the severely reduced phonon thermal conductivity of dielectrics and semiconductors [1-3]. The underlying mechanism is attributed to the increasing or even dominant boundary and interface scattering of phonons at micro- and nanoscale, which have been widely studied in the past decades [4-9]. As a potential avenue to alleviate this situation, phonon polaritons have been proposed to enhance the heat conduction along polar materials and nanostructures [10, 11]. For instance, in recent experimental studies, the hyperbolic phonon polaritons were shown to contribute to ~27% and ~60% of the total out-of-plane thermal conductivity of respectively bulk h-BN [12] and α -MoO₃ [13] at ~600 K.

Surface phonon polaritons (SPhPs) are surface electromagnetic waves coupled with optical lattice vibration (i.e. phonons) in polar materials [14-16]. The enhanced SPhP contribution to the in-plane heat conduction arises from the weaker energy absorption of surface waves propagating along thinner films that allow longer propagation lengths. The SPhP thermal conductivity is thus expected to increase as the film thickness decreases [10], which is opposite to the trend of the usual phonon counterpart. As a result, SPhPs become powerful heat carriers able to counteract the reduction of phonon heat conduction in semiconductor nanostructures, and provide a promising avenue to alleviate the heat dissipation problem in nano-electronics. Since the pioneering work [10], there have been a lot of theoretical investigations of SPhP heat transport along polar nanostructures, including thin films [17-24], nanowires [25, 26], nanoparticle chains and crystals [27-29].

In contrast, the experimental observation of the in-plane SPhP heat transport has been achieved over the last few years only. The increasing thermal conductivity of silica nanofilms for decreasing thicknesses [30] was measured with relatively large experimental uncertainties. Some of the co-authors also showed a decisive experimental evidence of the SPhP heat conduction through the increasing thermal conductivity with the temperature of sufficiently-thin amorphous silicon nitride (SiN) films [31]. More recently, some of us further reported the observation of the quasi-ballistic heat transport of SPhPs propagating over hundreds of micrometers [32]. Similar SPhP-mediated enhancements for the in-plane thermal diffusivity

of amorphous silicon carbon nanofilms supported on silicon were also observed [33], along with the enhanced thermal conductivity of metallic nanofilms supporting the propagation of surface plasmon polaritons (SPPs) [34, 35]. It is noteworthy to mention that remarkable heat conduction via SPhPs was also observed very recently along 3C-SiC nanowires with a gold coating serving as an efficient SPhP launcher on their ends [36]. Similar strategies were adopted by designing efficient SPhP absorbers on the ends of SiO₂ nanoribbons, which support noticeable SPhP heat conduction [37, 38]. These delicate experimental studies are outside the scope of the present work focused on nanofilms with length and width much larger than the thickness.

The theoretical interpretation of the observed in-plane SPhP heat transport remains, however, not fully established. The SPhP thermal conductivity has been usually computed with a diffusive model [10] involving an effective propagation length limited by the boundary scattering and given by the empirical Matthiessen's law [30-32]. In addition, only the SPhP contribution was evaluated [31, 32], and a direct comparison to the measured overall thermal conductivity (including both SPhP and phonon contribution) is still missing.

The aim of this work is to provide a better theoretical explanation of the experimental data of thermal conductivity by using a transport model coupling the dynamics of SPhPs and phonons propagating along polar thin films [20]. The transport model includes a direct numerical solution of Boltzmann transport equation (BTE) for SPhPs and heat diffusion equation for phonons. Thus we enable to separately quantify the contributions of multiple heat carriers (phonons and SPhPs) to the thermal conductivity of polar nanostructures. The remaining of the present work is organized as follows. The physical and mathematical models are introduced in Section 2, whereas Section 3 contains the description and discussion of the theoretical results in comparison with experiments. The concluding remarks are finally made in Section 4.

2. Physical and Mathematical Models

In this section, we will introduce the physical model of heat transport along polar dielectric nanofilms, together with the model of coupled phonons and SPhPs in Subsection

2.1. The numerical scheme to solve the coupled transport model is then presented in Subsection 2.2.

2.1 Physical model and mathematical description

We consider the in-plane heat transport along a polar dielectric thin film with a length L and thickness d , as shown in Figure 1. The heat conduction along this film is driven by two heat carriers: phonons due to lattice vibration, and SPhPs thermally excited by the motion of dipoles inside the polar medium. The excitation of SPhPs depends on the local thermal environment (i.e., local temperature) determined by the lattice vibration, whereas the local temperature is conversely impacted by the absorption (into heat) of surface electromagnetic waves. In other words, the dynamics of SPhPs and phonons are coupled with each other [20]. This is a crucial original feature of the present model compared to previous ones [17, 18, 23, 31, 32], which consider only the SPhP contribution to heat transport. The in-plane SPhP heat conduction considered in the present study is essentially two-dimensional (2D) [30] due to the following reasons: (i) both the length and width of the thin film are much larger than its thickness, and (ii) the wavelengths of SPhPs are generally much larger than the film thickness.

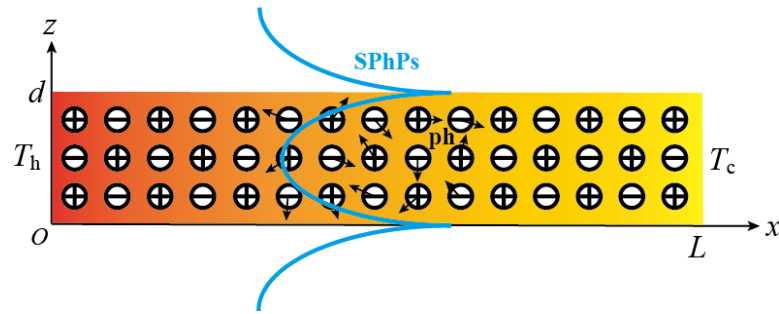


Figure 1. Schematic of heat transport along a polar dielectric nanofilm via lattice vibration (i.e. phonons, ph) and surface phonon polaritons (SPhPs). The length and thickness of the thin film are L and d respectively, whereas its width is infinite. The temperatures of the hot side and cold side are T_h and T_c respectively.

As the intrinsic propagation length (i.e. mean free path) of SPhPs is usually larger than the typical length of the nanofilms [10, 17, 20], the quasi-ballistic effect becomes important in SPhP heat transport. Therefore, the steady-state BTE under the relaxation time approximation is employed [10]:

$$\boldsymbol{\Omega} \cdot \nabla f_{\omega} = \frac{f_{\omega}^0(T) - f_{\omega}}{\Lambda_{\omega}}, \quad (1)$$

where $\boldsymbol{\Omega}$ is the unit direction vector, f_{ω} is the SPhP distribution function with $f_{\omega}^0(T)$ the Bose-Einstein equilibrium distribution at T , and Λ_{ω} is the frequency-dependent intrinsic propagation length. The phonon mean free path is usually much smaller than the film length and considerably larger than its thickness, inferring Casimir diffusive heat conduction [39] along the nanofilm. Thus the Fourier's law with an effective thermal conductivity κ_{ph} is adopted for phonons [20]:

$$\mathbf{q}_{\text{ph}} = -\kappa_{\text{ph}} \nabla T. \quad (2)$$

The overall heat flux along the thin film includes the contribution from both SPhPs and phonons ($\mathbf{q}_t = \mathbf{q} + \mathbf{q}_{\text{ph}}$), and satisfies the energy balance equation:

$$\nabla \cdot \mathbf{q}_t = 0, \quad (3)$$

where the SPhP heat flux is computed from the distribution function solution of Eq. (1):

$$\mathbf{q} = \frac{1}{4\pi^2 d} \int \mathbf{v}_g \hbar \omega f_{\omega} d\boldsymbol{\beta}_R. \quad (4)$$

In Eq. (4), \mathbf{v}_g and $\boldsymbol{\beta}_R$ denote the group velocity and the real part of in-plane wave vector of SPhPs respectively.

For convenience, the SPhP BTE in Eq. (1) is reformulated into a deviational intensity form [20]:

$$\boldsymbol{\Omega} \cdot \nabla \phi_{\omega} = \frac{\phi_{\omega}^0(T) - \phi_{\omega}}{\Lambda_{\omega}}, \quad (5)$$

where the deviational intensity distribution [40] of SPhPs is defined as: $\phi_{\omega} = I_{\omega} - I_{\omega}^0(T_0)$, with the intensity distribution: $I_{\omega} = v_g \hbar \omega f_{\omega} D(\omega)/2\pi$ and its equilibrium counterpart $I_{\omega}^0(T_0)$ at the system average temperature T_0 . The density of states of SPhPs per unit frequency per unit area is denoted by $D(\omega)$. The SPhP heat flux in Eq. (4) is reformulated into:

$$\mathbf{q} = \frac{1}{d} \int \int \boldsymbol{\Omega} \phi_{\omega} d\theta d\omega. \quad (6)$$

As we aim to provide a theoretical explanation of previous experimental results [31, 32], the 2D SPhP heat conduction is further simplified into a one-dimensional (1D) problem

limited by the film length only. This simplification is justified by the heat transfer between the uniformly-heated heater wire and the sensor wire in 3ω setup [32] or the radial heat dissipation from the laser-heated spot in micro time domain thermoreflectance (TDTR) setup [31]. As a result, the following 1D governing equations are obtained:

$$\mu \frac{\partial \phi_\omega}{\partial x} = \frac{\phi_\omega^0(T) - \phi_\omega}{\Lambda_\omega}, \quad (7)$$

$$q = \frac{1}{d} \iint \mu \phi_\omega d\theta d\omega, \quad (8)$$

$$0 = \kappa_{\text{ph}} \frac{\partial^2 T}{\partial x^2} + S(x), \quad (9)$$

In Eqs. (7) and (8), $\mu = \cos \theta$ denotes the directional cosine, with $\theta \in [0, 2\pi]$ the angle between the SPhP velocity direction and x -axis. Equation (9) is obtained by putting Eq. (2) into Eq. (3), and $S(x) = -\partial q / \partial x$ represents an effective heat source term due to the local absorption of SPhPs along the polar medium. To solve the governing equations, the following isothermal boundary conditions are supplemented:

$$\begin{cases} x = 0, T = T_h, \phi_\omega(\mu > 0) = v_g \frac{C_\omega}{2\pi} (T_h - T_0) \\ x = L, T = T_c, \phi_\omega(\mu < 0) = v_g \frac{C_\omega}{2\pi} (T_c - T_0) \end{cases}, \quad (10)$$

where the equilibrium deviational intensity distribution has been linearized when the temperature difference along the thin film is small, and $C_\omega = \hbar \omega \partial f_\omega^0 / \partial T D(\omega)$ is the spectral heat capacity.

As inputs into the BTE, we use the following real and imaginary parts of the in-plane wave vector $\beta = \beta_R + i\beta_I$ of SPhPs propagating along a dielectric film in small-thickness limit [17, 41]:

$$\beta_R = \sqrt{\varepsilon_1} k_0 \left[1 + \frac{\varepsilon_1 (k_0 d)^2}{8} \left(1 - \frac{2\varepsilon_1 \varepsilon_R}{|\varepsilon_2|^2} + \frac{\varepsilon_1^2 (\varepsilon_R^2 - \varepsilon_I^2)}{|\varepsilon_2|^4} \right) \right], \quad (11)$$

$$\beta_I = \sqrt{\varepsilon_1} k_0 \frac{(k_0 d)^2}{4} \frac{\varepsilon_1 \varepsilon_I}{|\varepsilon_2|^2} \left(1 - \frac{\varepsilon_1 \varepsilon_R}{|\varepsilon_2|^2} \right). \quad (12)$$

The complex dielectric function of the polar nanofilm as an active medium is $\varepsilon_2 = \varepsilon_R + i\varepsilon_I$, whereas the dielectric function of the in-active surrounding medium (vacuum in this work) is ε_1 . The light wave vector in vacuum is $k_0 = \omega/c$, with c the speed of light in vacuum. The dispersion relation of SPhPs along a dielectric film in Eqs. (11) and (12) represent the thin-film limit of the following general relation [41]:

$$\tanh\left(\frac{p_2 d}{2}\right) = -\frac{p_1 \varepsilon_2}{p_2 \varepsilon_1}, \quad (13)$$

where the transverse wave vectors are defined as: $p_j^2 = \beta^2 - \varepsilon_j k_0^2$, $j=1,2$. We focus on very thin nanofilms with significant enhancement of SPhP thermal conductivity, which decreases as the thickness increases and reaches its bulk limit [10, 17]. The 2D density of states of SPhPs in polar nanofilm is calculated by: $D(\omega) = \beta_R / 2\pi v_g$ [42], while their propagation length is determined by the imaginary part of in-plane wave vector as follows [10, 43]:

$$\Lambda_\omega = \frac{1}{2\beta_I}. \quad (14)$$

2.2 Numerical solution

The coupled heat transport via SPhPs and phonons along the polar nanofilm is resolved through a self-consistent numerical solution of Eqs. (7)-(9) with the boundary conditions in Eq. (10). The discrete-ordinate method (DOM) [44, 45] is adopted to solve the SPhP BTE in Eq. (7). Note that the DOM scheme was initially developed by Chandrasekhar [46] to solve the radiative transfer equation based on the idea of Wick [47]. The finite difference method (FDM) is employed to solve the heat diffusion equation (9). In the following, we briefly introduce the idea and procedure of the numerical scheme [20].

First, we explain the DOM scheme to solve the SPhP BTE for the deviational intensity distribution which is dependent on position, direction and frequency. The full plane angle of 2π and the full SPhP spectrum are respectively discretized into specific numbers of angular and spectral intervals. In this way, the SPhP intensity distribution becomes dependent on the discrete directions and frequencies. The macroscopic variables such as the heat flux in Eq. (8) are thus calculated by the following numerical integration:

$$q = \frac{\Delta\omega}{d} \frac{1}{2} \pi \sum_n \sum_k \mu_k (\phi_\omega)_n^k w_k. \quad (15)$$

In Eq. (15), the rectangular scheme is adopted for the spectral integration with an interval of $\Delta\omega$, whereas the Gauss-Legendre quadrature is adopted for the angular integration with a weight coefficient w_k . The indexes for spectral and angular nodes are $n=1,2,\dots,N_m$ and $k=1,2,\dots,N_\theta$ respectively, with N_m and N_θ the total number of spectral and angular nodes separately. The discrete form of SPhP BTE in Eq. (7) thus becomes:

$$\mu_k \frac{\partial (\phi_\omega)_n^k}{\partial x} = \frac{(\phi_\omega^0)_n - (\phi_\omega)_n^k}{(\Lambda_\omega)_n}. \quad (16)$$

In terms of the position discretization, various methods are available, such as the finite volume method (FVM) and FDM, with the latter adopted in this work. The step scheme [20, 44] is adopted for the spatial discretization, such that for $\mu_k > 0$, Eq. (16) becomes:

$$\mu_k \frac{(\phi_\omega)_{n,i}^k - (\phi_\omega)_{n,i-1}^k}{\Delta x} = \frac{(\phi_\omega^0)_{n,i} - (\phi_\omega)_{n,i}^k}{(\Lambda_\omega)_n}, \quad (17)$$

where Δx is the spatial step, and $i=1,2,\dots,N_x+1$ is the index of spatial node, with N_x+1 the total number of spatial nodes. From Eq. (17), the deviational intensity field for $\mu_k > 0$ is updated in a forward way from the left isothermal boundary:

$$(\phi_\omega)_{n,i}^k = \frac{m_n^k (\phi_\omega)_{n,i-1}^k + (\phi_\omega^0)_{n,i}}{m_n^k + 1}, \quad (18)$$

where the coefficient $m_n^k = \mu_k (\Lambda_\omega)_n / \Delta x$ is defined for short. The solution of the deviational intensity field for $\mu_k < 0$ is similar in a backward way from the right isothermal boundary [20]. Once the deviational intensity distribution is resolved, the SPhP heat flux is computed by Eq. (15). Then the effective heat source term due to SPhPs $S(x) = -\partial q / \partial x$ is calculated based on a second-order difference scheme for the spatial derivative of heat flux [20].

Once the effective heat source term is determined, the heat diffusion equation (9) is solved through a second-order FDM scheme as follows:

$$0 = \kappa_{\text{ph}} \frac{T_{i+1} + T_{i-1} - 2T_i}{(\Delta x)^2} + S_i. \quad (19)$$

In Eq. (19), for simplicity, we have used the same spatial grid as that in solving the SPhP BTE. With a careful treatment of the boundary conditions, the following algebraic equation set is obtained:

$$\mathbf{A}[T] = [b], \quad (20)$$

where $[T]$ is the column vector of discrete temperature distribution, whereas \mathbf{A} and $[b]$ are the coefficient matrix of dimension $(N_x + 1) \times (N_x + 1)$ and right column vector of dimension $(N_x + 1) \times 1$ respectively:

$$\mathbf{A} = \begin{bmatrix} -2 & 1 & & & \\ 1 & -2 & 1 & \mathbf{0} & \\ & \ddots & \ddots & \ddots & \\ & \mathbf{0} & 1 & -2 & 1 \\ & & & 1 & -2 \end{bmatrix}, [b] = \begin{bmatrix} -(\Delta x)^2 S_1 / \kappa_{\text{ph}} - T_h \\ \vdots \\ -(\Delta x)^2 S_i / \kappa_{\text{ph}} \\ \vdots \\ -(\Delta x)^2 S_{N_x+1} / \kappa_{\text{ph}} - T_c \end{bmatrix}. \quad (21)$$

The lattice temperature distribution along the polar thin film is resolved just by a matrix inversion: $[T] = \mathbf{A}^{-1}[b]$.

The numerical solution of SPhP BTE is done again with the equilibrium deviational intensity updated by the temperature distribution solution of heat diffusion equation. This iterative procedure is repeated in a self-consistent way until the relative difference of the macroscopic variables (temperature and heat flux distributions) between two iteration steps is less than 10^{-8} , as summarized in Figure 2. Once the convergence is achieved, both the deviational intensity distribution function of SPhPs and the lattice temperature distribution are finally resolved. Therefore, the SPhP and phonon heat fluxes as well as the overall heat flux are obtained. The SPhP and phonon heat fluxes might vary with position along the thin film due to their mutual energy exchange, while the overall heat flux $q_t = q + q_{\text{ph}}$ must be independent of position as required by Eq. (3). The overall thermal conductivity of the thin film is calculated based on: $\kappa_t = q_t L / (T_h - T_c)$, and the SPhP contribution is then extracted by:

$$\kappa_{\text{SPhP}} = \kappa_t - \kappa_{\text{ph}}.$$

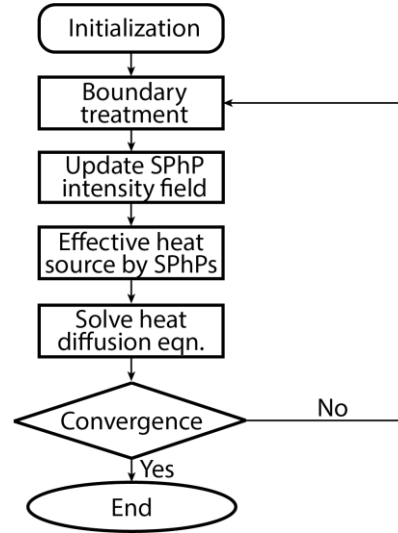


Figure 2. Iteration procedure of the coupled SPhP-phonon heat transport model

3. Results and Discussions

In this section, we will employ the theoretical model in Section 2 to interpret the experimental results of heat conduction in polar dielectric nanofilms. In Section 3.1, the SPhP properties and transport features relevant to experiments are introduced. The explanation of two sets of experimental results using different techniques will be presented in Section 3.2 and Section 3.3 respectively. Finally, we provide discussions and perspectives about the coupled dynamics of SPhPs and phonons, as well as the validity of kinetic theory for SPhP heat transport.

3.1 SPhP properties and transport features

In this work, we will explain the experimental result of thermal conductivity of amorphous SiN nanofilms [31, 32]. The measured dielectric function of SiN, which is practically independent of temperature from 300 K to 800 K [31], is adopted for modeling, as given in Figure 3(a). The dispersion relation and propagation length of SPhPs in SiN nanofilms with thicknesses of 30 nm and 50 nm are calculated based on Eqs. (11), (12) and (14), as shown in Figure 3(b) and Figure 3(c). Note that the dispersion relation of SPhPs in very thin polar film is quite close to that of the light line, which is consistent with previous

predictions [17, 23, 24]. On the other hand, the SPhP propagation length is rather long and can even reach meter-scale at low frequency, due to low energy absorption.

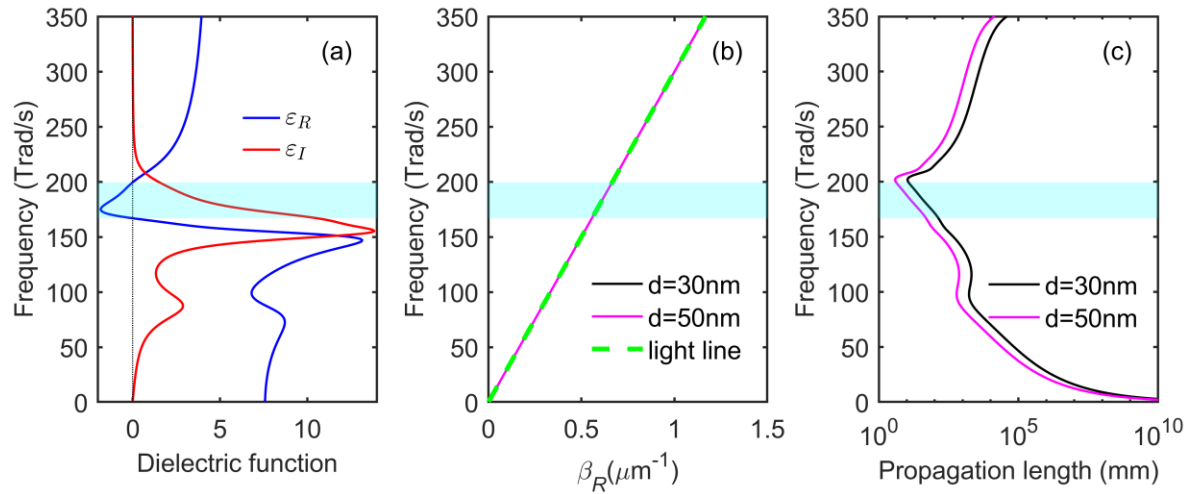


Figure 3. SPhP properties in SiN nanofilms: (a) dielectric function, with real part ϵ_R and imaginary part ϵ_I ; (b) dispersion relation, with β_R the real part of the wave vector; (c) SPhP propagation length. The shaded region represents the Reststrahlen band with negative ϵ_R .

The SPhPs are usually thought to be supported within the Reststrahlen band where $\epsilon_R < 0$ [15, 16]. For polar dielectric crystals, this band lies between the frequencies of transverse optical (TO) and longitudinal optical (LO) phonons. For the polar amorphous SiN considered in the present work, the Reststrahlen band just lies in the frequency range with negative ϵ_R , as illustrated by the shaded region in Figure 3(a). This rigorous definition of SPhPs is based on the real dispersion relation of surface waves in lossless media (i.e. $\epsilon_I = 0$) [41]. However, a much broader spectrum of surface waves or surface polaritons can be supported along lossy polar thin films with finite ϵ_I , as demonstrated in previous theoretical calculation [41] and direct experimental detection [48]. The coupled surface waves along a polar thin film exist as long as the real part of the transverse wave vector is positive (i.e. $p_{1R} > 0$) [41]. To provide an intuitive understanding, we show the transverse decay length ($L_p = 1/p_{1R}$) and transverse confinement rate ($\delta = L_p/\lambda_p$, with $\lambda_p = 1/p_{1I}$ [30]) of surface waves along SiN nanofilms in Figure 4(a) and Figure 4(b) respectively. The expressions of p_{1R} and p_{1I} can be found in previous works [31, 41]. One can see well-bounded surface waves are supported in a very

broad spectrum beyond the Reststrahlen band. The contribution of those thermally excited broadband SPhPs to in-plane heat transport will be quantified later in this work.

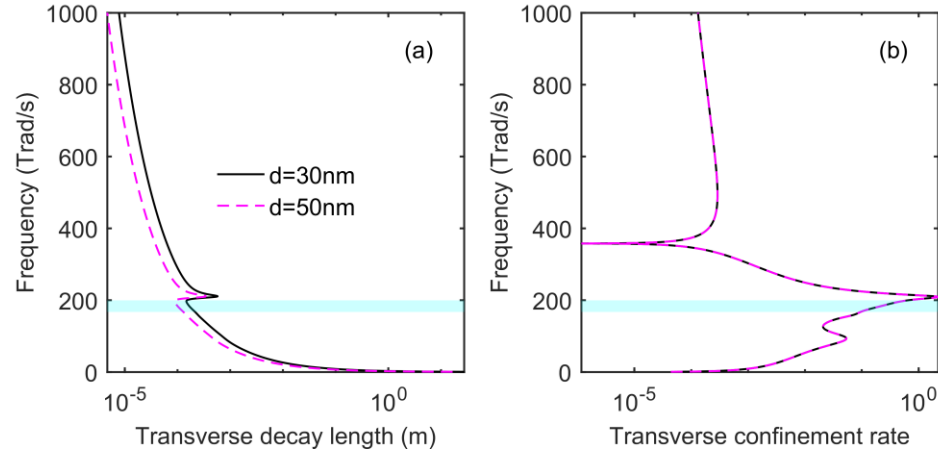


Figure 4. Propagation parameters of coupled surface waves along SiN nanofilms: (a) transverse decay length and (b) transverse confinement rate in the surrounding vacuum. The shaded region represents the Reststrahlen band.

As SiN in its amorphous phase is considered here, the lattice periodicity breaks down and the concept of ‘phonons’ remains debated. More relevant heat carriers have been proposed in amorphous systems, including propagons and diffusons [49, 50]. However, for simplicity and generality, we keep using the term ‘phonons’, which is true in crystalline polar nanostructures [36] and refers to more precisely ‘lattice vibration’ in amorphous materials. In the present modeling of heat transport in amorphous SiN nanofilms, we also assume a constant phonon thermal conductivity, i.e. independent of temperature. This assumption is justified by previous observations [31, 32]: the thermal conductivity of SiN film with a thickness of 200 nm decreases with increasing temperature due to intrinsic phonon scattering; it becomes almost temperature-independent at a film thickness of 100 nm, where the SPhP contribution is still negligible. In a deeper view, the temperature dependence of diffuson contribution is negligible, whereas the propagon contribution is suppressed by the boundary scattering in such nanofilm (< 100 nm) and is also temperature-independent [31].

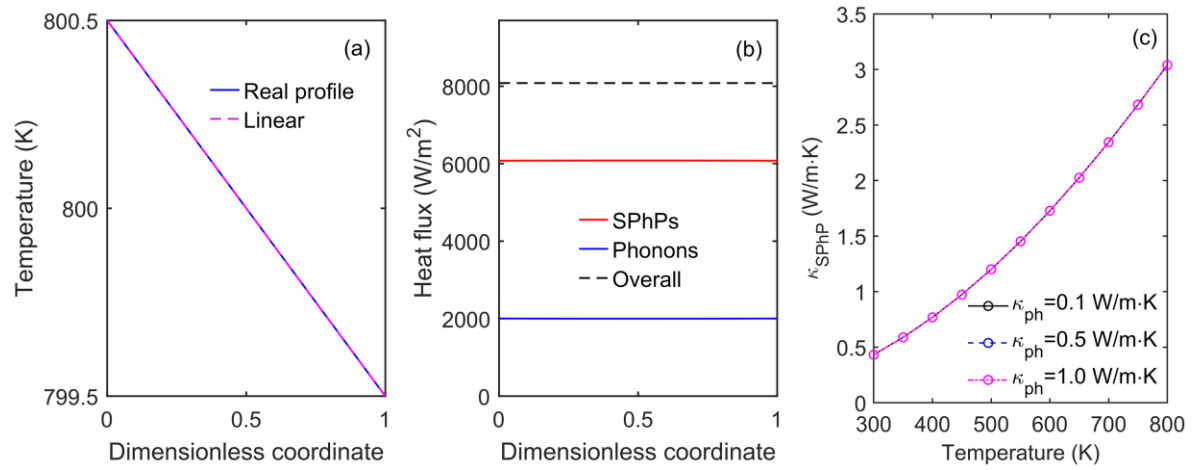


Figure 5. Quasi-ballistic transport behavior of SPhPs along SiN thin film with $d = 30$ nm and $L = 500$ μm : (a) temperature and (b) heat flux distributions around 800 K when $\kappa_{\text{ph}} = 1.0$ W/m \cdot K; (c) SPhP thermal conductivity at three different κ_{ph} .

To illustrate the coupling physical features in heat transport along SiN thin films with relevant lengths less than 1 mm in experiments [31, 32], we present the modeling result in a 500- μm -long and 30-nm-thick thin film in Figure 5. The average system temperature is set at 800 K, as the highest temperature in the recent experiment [31], where the contribution of SPhPs is most enhanced. A small temperature difference of 1 K is exerted on both ends of the thin film. As is shown in Figure 5(a), the lattice temperature distribution profile is almost linear, inferring that the effective heat source term from SPhPs in the heat diffusion equation (9) is very small. This is indeed the case as seen in the flat profile of the SPhP heat flux distribution in Figure 5(b), where the gradient $-\partial q/\partial x$ is close to zero. It infers only tiny mutual energy exchange between SPhPs and phonons, as the SPhP propagation length is much longer than the film length such that the SPhPs transport quasi-ballistically along the nanofilm with negligible absorption by the polar lattice. As a result, the SPhP thermal conductivity is pretty much independent of the phonon counterpart, as shown in Figure 5(c). Essentially, the right-hand term in the SPhP BTE in Eq. (7) is vanishingly small in this situation. Therefore, the coupling between SPhPs and phonons in the experimental conditions [31, 32] is generally weak. However, for thin films with a longer length comparable to the SPhP propagation length, the SPhPs will couple more strongly with phonons, as to be further discussed later.

3.2 Explanation of 3ω experimental result

We now employ our theoretical model to explain the experimental data of thermal conductivity of SiN nanofilms in Ref. [32]. First, we model the heat transport along SiN thin films with a thickness of 30 nm and two lengths of 100 μm and 200 μm . The SPhP thermal conductivity is independent of the assigned phonon counterpart, attributed to the quasi-ballistic transport behavior of SPhPs. Therefore, the phonon thermal conductivity could be extracted by fitting the calculated overall thermal conductivity to the measured one in Ref. [32]. In this way, the theoretical model with $\kappa_{\text{ph}} = 1.42 \text{ W/m}\cdot\text{K}$ is able to explain appreciably well the measured temperature-dependent thermal conductivity of thin films with both lengths, as shown in Figure 6(a) and Figure 6(b). The enhancement of thermal conductivity from $L = 100 \mu\text{m}$ to $L = 200 \mu\text{m}$ fully comes from the contribution of SPhPs, as the phonon contribution is the same for the two cases.

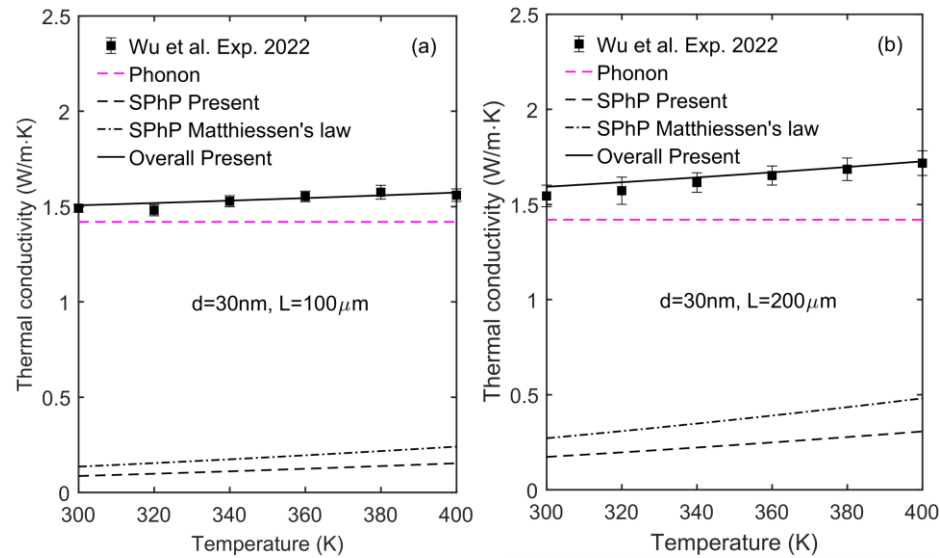


Figure 6. Temperature-dependent thermal conductivity of SiN thin film with a thickness of 30 nm and two lengths: (a) $L = 100 \mu\text{m}$; (b) $L = 200 \mu\text{m}$. The filled squares with errorbar denote the experimental data from Ref. [32], the magenta dashed line, black dashed line and solid line represent respectively the phonon, SPhP, and overall thermal conductivity by the present model, whereas the dash-dotted line represents the SPhP thermal conductivity based on the Matthiessen's law.

Also we compare to the predicted SPhP contribution based on the bulk thermal conductivity formula [10]:

$$\kappa_{\text{SPhP}} = \frac{1}{4\pi d} \int \hbar \omega \frac{\partial f_{\text{eq}}}{\partial T} \Lambda_{\text{eff}} \beta_R d\omega, \quad (22)$$

where the effective propagation length is computed by the empirical Matthiessen's law [32]:

$$\frac{1}{\Lambda_{\text{eff}}} = \frac{1}{\Lambda_{\omega}} + \frac{1}{L}. \quad (23)$$

Although Eq. (22) seems to capture the main trend of temperature-dependent SPhP thermal conductivity, it overestimates considerably its absolute value and thus will underestimate the phonon contribution. The present direct numerical solution of SPhP BTE provides a more accurate account of the boundary scattering of SPhPs compared to the empirical treatment in Eq. (23), as also emphasized in a recent numerical study in silica thin films [23].

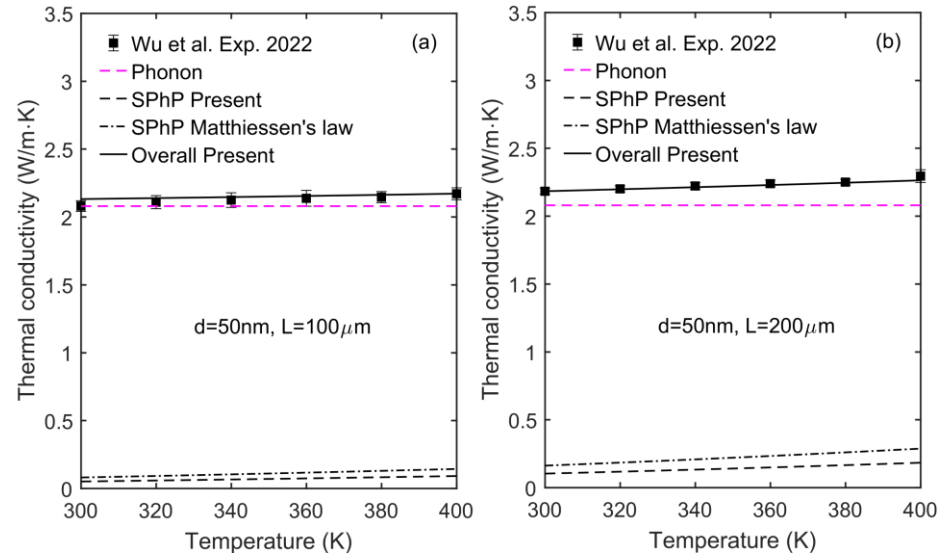


Figure 7. Temperature-dependent thermal conductivity of SiN thin film with a thickness of 50 nm and two lengths: (a) $L = 100 \mu\text{m}$; (b) $L = 200 \mu\text{m}$. The filled squares with errorbar denote the experimental data from Ref. [32], the magenta dashed line, black dashed line and solid line represent respectively the phonon, SPhP, and overall thermal conductivity by the present model, whereas the dash-dotted line represents the SPhP thermal conductivity based on the Matthiessen's law.

We also obtain a good fitting of the measured thermal conductivity of SiN thin films with a thickness of 50 nm and two lengths of $100 \mu\text{m}$ and $200 \mu\text{m}$, as shown in Figure 7(a) and Figure 7(b). Again, the theoretical model with a single $\kappa_{\text{ph}} = 2.08 \text{ W/m}\cdot\text{K}$ is able to explain the enhancement of thermal conductivity from $L = 100 \mu\text{m}$ to $L = 200 \mu\text{m}$ fully attributed to SPhPs. Compared to the 30 nm thin film, the SPhP thermal conductivity of the 50 nm thin film is smaller due to shorter propagation length as given in Figure 3(c). In

contrast, the phonon thermal conductivity is higher in this thicker film due to less boundary scattering of phonons. This demonstrates the opposite trends of size effect in phonon and SPhP heat transport along the in-plane direction of thin films. In contrast to the previous study only calculating the enhanced contribution to heat conduction by SPhPs [32], the present work provides a consistent theoretical explanation of the experimental data of overall absolute thermal conductivity. Furthermore, the quantified phonon thermal conductivity will establish reference data for investigating the size effect in vibrational heat transport along amorphous nano-structures which remains still an open question [51, 52].

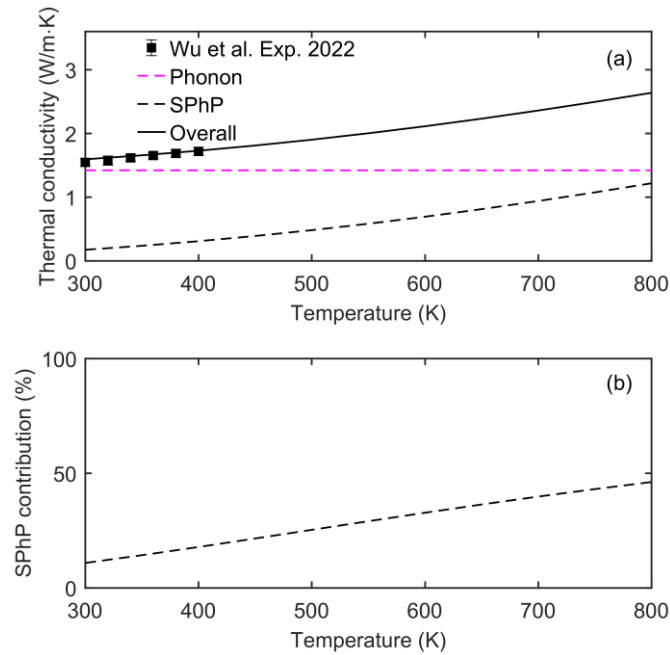


Figure 8. Temperature-dependent heat transport along SiN thin film with a thickness of 30 nm and a length of 200 μm : (a) thermal conductivity, the lines represent the theoretical calculation whereas the symbols with errorbar denote the experimental data from Ref. [32]; (b) the relative contribution of SPhPs.

The contribution of SPhPs to heat transport along polar thin films is known to increase as the temperature increases. As the highest temperature in the experiment [32] is only up to 400 K, the ratio of SPhP thermal conductivity over the overall one is less than 20% in Figure 6 and Figure 7. To demonstrate a more significant contribution of SPhPs, we also predict the thermal conductivity of the SiN thin film with a thickness of 30 nm and a length of 200 μm [32] up to a much higher temperature of 800 K, as shown in Figure 8. As seen in Figure 8(a),

the SPhP thermal conductivity increases a lot as the temperature is elevated from 300 K to 800 K. This is mainly caused by the increasing population of SPhPs in higher-frequency range at higher temperatures. The spectral contribution of thermally excited SPhPs to the thermal conductivity will also be broadened to higher-frequency range, as clearly shown in Figure 9. As a result, the SPhP thermal conductivity becomes comparable to the phonon counterpart, as is more explicitly illustrated in Figure 8(b), where the SPhP contribution is close to half of the total thermal conductivity at 800 K. Such stronger evidence of in-plane SPhP heat transport is pending to be observed by the 3ω setup [32] once the high-temperature measurement is feasible.

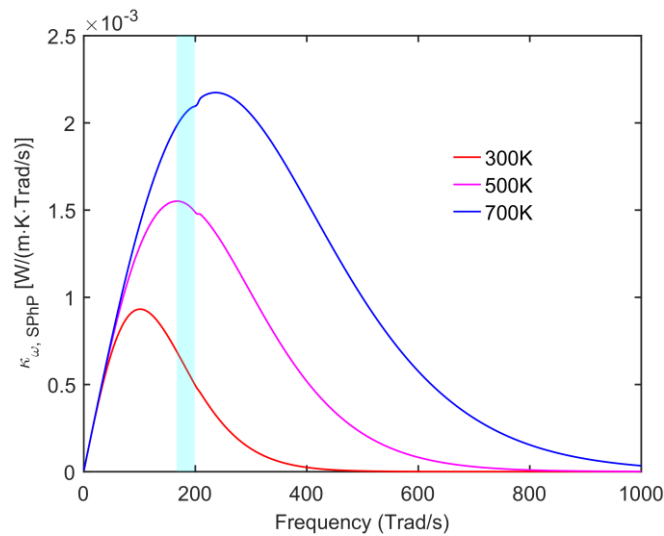


Figure 9. Spectral thermal conductivity of surface phonon polaritons (SPhPs) along SiN thin film with a thickness of 30 nm and a length of 200 μm at various temperatures. The shaded region represents the Reststrahlen band.

3.3 Explanation of TDTR experimental result

Then we would like to discuss the theoretical explanation of the experimental data of thermal conductivity of SiN thin films in Ref. [31]. The thermal conductivity was measured by TDTR setup, with nine aluminum (Al) pads deposited as transducers in a 3×3 array on the SiN thin films. The SiN thin films with a thickness of 50 nm and 30 nm are suspended on a $1 \text{ mm} \times 1 \text{ mm}$ and $0.5 \text{ mm} \times 0.5 \text{ mm}$ square windows of silicon substrate respectively [31]. The SPhP and phonon heat transport from the laser-heated transducers to the substrate is a complicated 2D process, such that our simplified 1D modeling might not work well.

However, we could still provide a semi-quantitative understanding of the experimental result by using an ‘effective’ 1D model with an effective thin film length. For the 50 nm thin film, the distances between the eight Al pads near the thin film edges and the substrate are scattered between $\sim 100\ \mu\text{m}$ and $\sim 170\ \mu\text{m}$, whereas the single center Al pad is $\sim 500\ \mu\text{m}$ away from the substrate. As the phonon thermal conductivity is unknown at this stage, we present a fitting of the enhanced thermal conductivity due to SPhPs in experiment $\Delta\kappa_{\text{SPhP}} = \kappa(T) - \kappa(300\text{K})$ by our calculated $\Delta\kappa_{\text{SPhP}} = \kappa_{\text{SPhP}}(T) - \kappa_{\text{SPhP}}(300\text{K})$ with effective film lengths from $100\ \mu\text{m}$ to $200\ \mu\text{m}$, following the strategy in Ref. [32]. With an effective length of $150\ \mu\text{m}$, our 1D theoretical model fits $\Delta\kappa_{\text{SPhP}}$ reasonably well as shown in Figure 10(a). In this way, the present theoretical model with $\kappa_{\text{ph}} = 0.22\ \text{W/m}\cdot\text{K}$ is able to fit the overall absolute thermal conductivity of 50 nm SiN thin film within the experimental uncertainty, as shown in Figure 11(a). As a comparison, the prediction based on the empirical Matthiessen’s law [i.e., Eqs. (22) and (23)] overrates not only the absolute value but also the increasing slope of the temperature-dependent SPhP thermal conductivity. It is crucial to use the direct numerical solution of SPhP BTE to compute more accurately its contribution to heat transport.

As for the 30 nm thin film, the distances between the eight Al pads near the thin film edges and the substrate are scattered between $\sim 50\ \mu\text{m}$ and $\sim 80\ \mu\text{m}$. The 1D theoretical model even with a minimal effective length of $50\ \mu\text{m}$ overestimates the enhanced thermal conductivity due to SPhPs, as seen in Figure 10(b). The observed enhancement of heat conduction due to SPhPs at 30 nm is smaller than that at 50 nm, which is opposite to the theoretical expectation. As a result, the present theoretical model is only able to provide a semi-quantitative fitting of the overall absolute thermal conductivity of 30 nm SiN thin film with $\kappa_{\text{ph}} = 0.08\ \text{W/m}\cdot\text{K}$, as seen in Figure 11(b). Although with a rough 1D approximation, our theoretical model still explains reasonably well the measured heat transport along SiN thin films [31]. The results also indicate the significance of boundary scattering in the suppression of SPhP heat transport. Indeed the efficient coupling between SPhPs and thermal reservoirs has been shown to boost the SPhP thermal conductivity of amorphous SiO_2 nanoribbons in recent experimental reports [37, 38]. The community is still awaiting for more measurements of thermal conductivity of polar dielectric thin films with relatively simple

configurations as in the 3ω setup [32], which would help a more clear understanding of the physics of coupled SPhP-phonon transport, as well as a further verification of the SPhP transport theory.

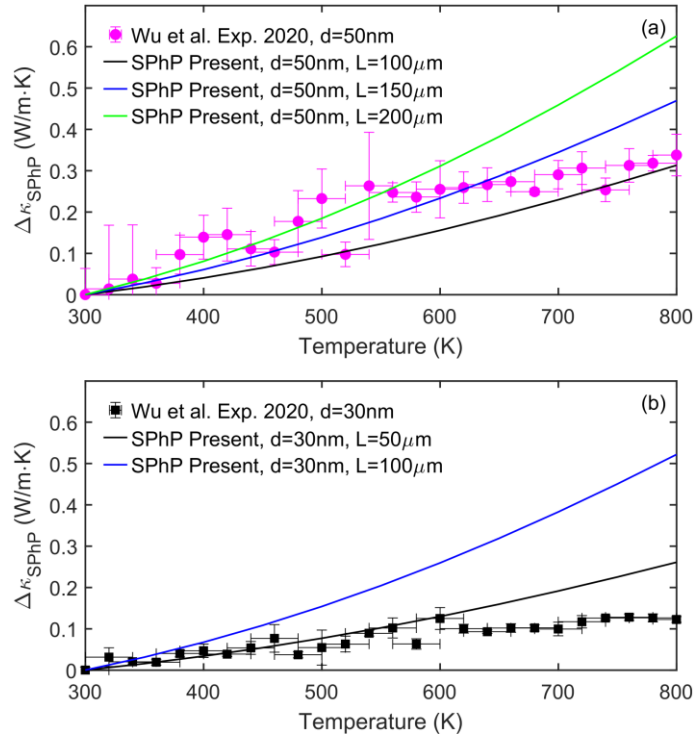


Figure 10. Enhanced thermal conductivity due to SPhPs in SiN thin film with two different thicknesses: (a) $d = 50$ nm; (b) $d = 30$ nm. The filled symbols with errorbar denote experimental data [$\Delta\kappa_{\text{SPhP}} = \kappa(T) - \kappa(300\text{K})$] from Ref. [31]. The solid lines denote the present modeling [$\Delta\kappa_{\text{SPhP}} = \kappa_{\text{SPhP}}(T) - \kappa_{\text{SPhP}}(300\text{K})$] with different effective film lengths.

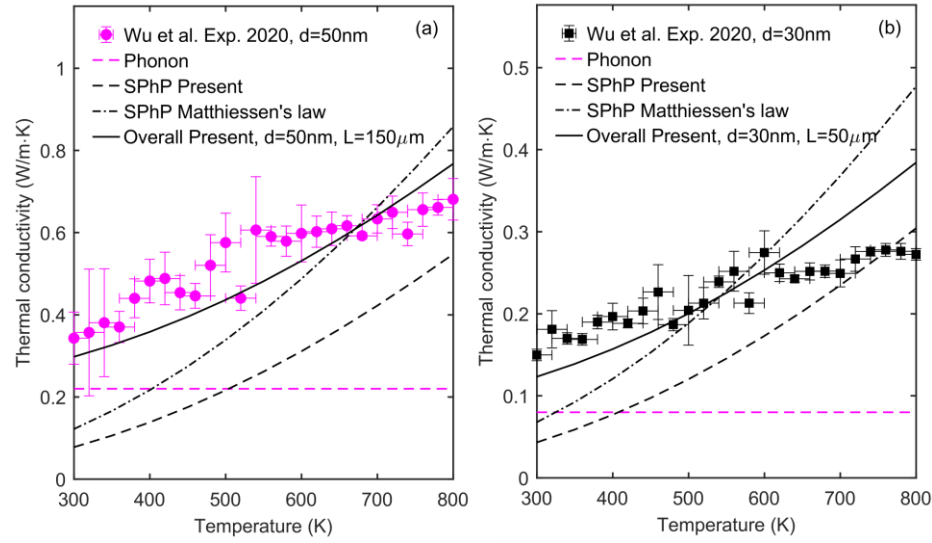


Figure 11. Temperature-dependent thermal conductivity of SiN thin film with two thicknesses: (a) $d = 50$ nm; (b) $d = 30$ nm. The filled symbols with errorbar denote experimental data from Ref. [31]. The lines in (a) denote theoretical modeling with $d = 50$ nm, $L = 150$ μ m, whereas the lines in (b) denote theoretical modeling with $d = 30$ nm, $L = 50$ μ m.

3.4 Discussions and perspectives

In our explanation of the 3ω and TDTR experimental results [31, 32] in Section 3.2 and Section 3.3, the in-plane heat conduction via SPhPs and phonons lies in the weakly coupling regime. Under this quasi-ballistic condition, the SPhP heat transport is practically independent of the phonon counterpart and could be determined by a direct numerical solution of the SPhP BTE only. This description represents an improvement over previous works [30-32] based on empirical models for the boundary scattering. By contrast, as the film length increases and becomes comparable to the propagation length of SPhPs, the lattice thermal adsorption of SPhPs along their propagation becomes significant. In this ballistic-diffusive regime, we have to consider the SPhP-phonon coupling, which gives rise to a nonlinear temperature profile as shown in Figure 12(a) for a SiN thin film with a thickness of 50 nm and a length of 20 μ m. The dominant emission or absorption of SPhPs within the first ($0 < x/L < 0.5$) or second ($0.5 < x/L < 1$) half of the nanofilm turns out to be an effective heat sink or source for phonon heat conduction. As a result, both the SPhP and phonon heat fluxes are no longer independent of position along the nanofilm, as shown in Figure 12(b). This fact indicates that the dynamics of both SPhPs and phonons have to be simultaneously

taken into account when evaluating the thermal conductivity of the nanofilm. Our coupled model thus provides a crucial tool for analyzing heat conduction in polar nanostructures via multiple heat carriers.

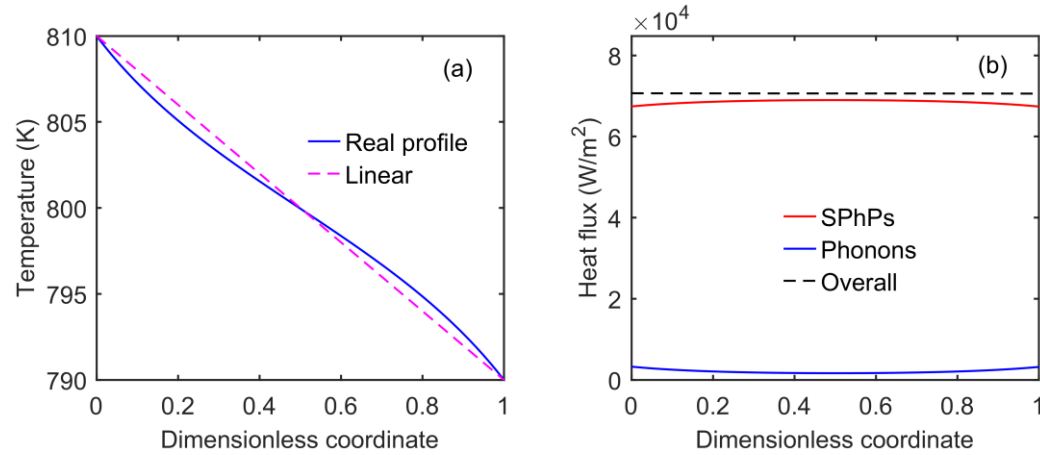


Figure 12. Coupled heat conduction via SPhPs and phonons along a SiN thin film with a thickness of 50 nm and a length of 20 nm: (a) temperature and (b) heat flux distributions. Calculations were done with a phonon thermal conductivity of $\kappa_{ph} = 2.08$ W/m·K from Section 3.2.

Finally, we would like to comment on the validity of kinetic theory of SPhPs, as the basis of our theoretical model. The comparison of the BTE prediction with that of fluctuational electrodynamics (FE) for the SPhP heat transport along polar thin films showed a favorable agreement [11]. The same comparison and agreement have been also reported in a recent study for the SPP heat transport along metallic thin films [34]. However, those comparisons are not fully rigorous since the physical models in FE and BTE calculations are slightly different. While the BTE calculation considers the presence of a smooth temperature gradient along a thin film, the FE one has been done by setting half of the thin film at a specific temperature and the other half at 0 K [11]. A rigorous FE modeling of in-plane SPhP heat conduction inside a dissipative thin film media is a challenging task, as tackled by a recent pioneering work [53]. The spectral thermal conductivity predicted by BTE for an infinitely long SiO₂ sheet with spatial periodicity agreed well with that by FE at different wave vectors down to a certain frequency, below which they disagree [53]. As the low-frequency regime typically involves long propagation length of SPhPs, a more rigorous examination of the kinetic theory should account for the finite length of the thin films. The

investigation of this size effect goes beyond the scope of this study and remains a formidable challenge. However, previous theoretical works [11, 34, 53] and the comparison of the present results with experimental data indicate that the kinetic theory captures the main trend and provides a quasi-quantitative description of heat conduction mediated by surface polaritons. Within the current state-of-art knowledge, the BTE formalism thus represents an indispensable theoretical tool for describing the not-so-well-explored heat conduction via SPhPs and SPPs, which are drawing more and more attention as novel channels for heat dissipation applications [34, 36-38].

4. Conclusions

We have developed a theoretical model for explaining the recently measured thermal conductivities of polar nanofilms supporting the propagation of surface phonon polaritons. Based on a direct numerical solution of Boltzmann transport equation for polaritons and heat diffusion equation for phonons, we have shown that the simultaneous and coupled dynamics of polaritons and phonons makes it possible to quantify their separate contributions to the total thermal conductivity. The weak coupling between polaritons and phonons in the nanofilm indicates significant suppression of the polariton heat transport by boundary scattering. The present study thus paves a way for the theoretical explanation of the enhanced heat conduction driven by the propagation of polaritons along various polar and metallic nanostructures, and also calls for more extensive experimental measurements of the polariton heat conduction in the future. Our work also promotes the understanding of the mesoscopic physics of thermal conductivity enhancement driven by SPhPs and its application in thermal management of micro- and nano-electronics.

Acknowledgements

This work was supported by the CREST JST (Grant Number JPMJCR19I1). Y. Guo also appreciates the financial support of the starting-up funding (AUGA2160500923) from Harbin Institute of Technology and the NSF Fund for Excellent Young Scientists Fund Program (Overseas).

Conflict of Interest

The authors have no conflicts to disclose.

Data Availability

The data that support the findings of this study are available from the corresponding author upon reasonable request.

References

- [1] L. Shi, C. Dames, J.R. Lukes, P. Reddy, J. Duda, D.G. Cahill, J. Lee, A. Marconnet, K.E. Goodson, J.-H. Bahk, Evaluating broader impacts of nanoscale thermal transport research, *Nanoscale and Microscale Thermophysical Engineering*, 19 (2015) 127-165.
- [2] M.S. Lundstrom, M.A. Alam, Moore's law: The journey ahead, *Science*, 378 (2022) 722-723.
- [3] D.-S. Tang, B.-Y. Cao, Phonon thermal transport and its tunability in GaN for near-junction thermal management of electronics: A review, *International Journal of Heat and Mass Transfer*, 200 (2023) 123497.
- [4] G. Chen, *Nanoscale energy transport and conversion: a parallel treatment of electrons, molecules, phonons, and photons*, Oxford University Press, New York, 2005.
- [5] Z.M. Zhang, *Nano/microscale heat transfer*, McGraw-Hill, New York, 2007.
- [6] D.G. Cahill, P.V. Braun, G. Chen, D.R. Clarke, S. Fan, K.E. Goodson, P. Keblinski, W.P. King, G.D. Mahan, A. Majumdar, H.J. Maris, S.R. Phillpot, E. Pop, L. Shi, *Nanoscale thermal transport. II. 2003-2012*, *Applied Physics Reviews*, 1 (2014) 011305.
- [7] Y. Guo, M. Wang, Phonon hydrodynamics and its applications in nanoscale heat transport, *Physics Reports*, 595 (2015) 1-44.
- [8] L. Qiu, N. Zhu, H. Zou, Y. Feng, X. Zhang, D. Tang, Advances in thermal transport properties at nanoscale in China, *International Journal of Heat and Mass Transfer*, 125 (2018) 413-433.
- [9] J. Chen, X. Xu, J. Zhou, B. Li, Interfacial thermal resistance: Past, present, and future, *Reviews of Modern Physics*, 94 (2022) 025002.
- [10] D.-Z.A. Chen, A. Narayanaswamy, G. Chen, Surface phonon-polariton mediated thermal conductivity enhancement of amorphous thin films, *Physical Review B*, 72 (2005) 155435.
- [11] D.-Z.A. Chen, G. Chen, Heat flow in thin films via surface phonon-polaritons, *Frontiers in Heat and Mass Transfer*, 1 (2010) 023005.
- [12] H. Salihoglu, V. Iyer, T. Taniguchi, K. Watanabe, P.D. Ye, X. Xu, Energy transport by radiation in hyperbolic material comparable to conduction, *Advanced Functional Materials*, 30 (2020) 1905830.
- [13] Y. Chen, M.A.S. Pacheco, H. Salihoglu, X. Xu, Greatly Enhanced Radiative Transfer Enabled by Hyperbolic Phonon Polaritons in α -MoO₃, *Advanced Functional Materials*, DOI (2024) 2403719.
- [14] K. Joulain, J.-P. Mulet, F. Marquier, R. Carminati, J.-J. Greffet, Surface electromagnetic waves thermally excited: Radiative heat transfer, coherence properties and Casimir forces revisited in the near field, *Surface Science Reports*, 57 (2005) 59-112.
- [15] S. Foteinopoulou, G.C.R. Devarapu, G.S. Subramania, S. Krishna, D. Wasserman, Phonon-polaritonics: enabling powerful capabilities for infrared photonics, *Nanophotonics*, 8 (2019) 2129-2175.
- [16] C.R. Gubbin, S. De Liberato, T.G. Folland, Surface phonon polaritons for infrared optoelectronics, *Journal of Applied Physics*, 131 (2022) 030901

- [17] J. Ordonez-Miranda, L. Tranchant, T. Tokunaga, B. Kim, B. Palpant, Y. Chalopin, T. Antoni, S. Volz, Anomalous thermal conductivity by surface phonon-polaritons of polar nano thin films due to their asymmetric surrounding media, *Journal of Applied Physics*, 113 (2013) 084311.
- [18] J. Ordonez-Miranda, L. Tranchant, Y. Chalopin, T. Antoni, S. Volz, Thermal conductivity of nano-layered systems due to surface phonon-polaritons, *Journal of Applied Physics*, 115 (2014) 054311.
- [19] M. Lim, J. Ordonez-Miranda, S.S. Lee, B.J. Lee, S. Volz, Thermal-conductivity enhancement by surface electromagnetic waves propagating along multilayered structures with asymmetric surrounding media, *Physical Review Applied*, 12 (2019) 034044.
- [20] Y. Guo, S. Tachikawa, S. Volz, M. Nomura, J. Ordonez-Miranda, Quantum of thermal conductance of nanofilms due to surface-phonon polaritons, *Physical Review B*, 104 (2021) L201407.
- [21] C. Huang, Y. Lan, Thermophysical study of surface phonon polaritons in multilayer systems for heat dissipation, *International Journal of Thermal Sciences*, 159 (2021) 106548.
- [22] S. Tachikawa, J. Ordonez-Miranda, Y. Wu, L. Jalabert, R. Anufriev, S. Volz, M. Nomura, In-plane surface phonon-polariton thermal conduction in dielectric multilayer systems, *Applied Physics Letters*, 121 (2022).
- [23] K.H. Yun, B.J. Lee, S.H. Lee, Modeling effective thermal conductivity enhanced by surface waves using the Boltzmann transport equation, *Scientific Reports*, 12 (2022) 15477.
- [24] S. Li, S. Shin, Long-Range Polaritonic Heat Conduction in Asymmetric Surrounding Media, *Journal of Applied Physics*, 134 (2023) 055101.
- [25] J. Ordonez-Miranda, L. Tranchant, B. Kim, Y. Chalopin, T. Antoni, S. Volz, Quantized thermal conductance of nanowires at room temperature due to Zenneck surface-phonon polaritons, *Physical Review Letters*, 112 (2014) 055901.
- [26] Y. Guo, M. Nomura, S. Volz, J. Ordonez-Miranda, Heat transport driven by the coupling of polaritons and phonons in a polar nanowire, *Energies*, 14 (2021) 5110.
- [27] J. Ordonez-Miranda, L. Tranchant, S. Gluchko, S. Volz, Energy transport of surface phonon polaritons propagating along a chain of spheroidal nanoparticles, *Physical Review B*, 92 (2015) 115409.
- [28] J. Ordonez-Miranda, L. Tranchant, K. Joulain, Y. Ezzahri, J. Drevillon, S. Volz, Thermal energy transport in a surface phonon-polariton crystal, *Physical Review B*, 93 (2016) 035428.
- [29] E.J. Tervo, B.A. Cola, Z.M. Zhang, Comparison of kinetic theory and fluctuational electrodynamics for radiative heat transfer in nanoparticle chains, *Journal of Quantitative Spectroscopy & Radiative Transfer*, 246 (2020) 106947.
- [30] L. Tranchant, S. Hamamura, J. Ordonez-Miranda, T. Yabuki, A. Vega-Flick, F. Cervantes-Alvarez, J.J. Alvarado-Gil, S. Volz, K. Miyazaki, Two-dimensional phonon polariton heat transport, *Nano Letters*, 19 (2019) 6924-6930.
- [31] Y. Wu, J. Ordonez-Miranda, S. Gluchko, R. Anufriev, D.D.S. Meneses, L. Del Campo, S. Volz, M. Nomura, Enhanced thermal conduction by surface phonon-polaritons, *Science Advances*, 6 (2020) eabb4461.
- [32] Y. Wu, J. Ordonez-Miranda, L. Jalabert, S. Tachikawa, R. Anufriev, H. Fujita, S. Volz, M. Nomura, Observation of heat transport mediated by the propagation distance of surface phonon-polaritons over hundreds of micrometers, *Applied Physics Letters*, 121 (2022) 112203.
- [33] S. Hamyeh, R. Tauk, P.-M. Adam, M. Kazan, Mid-IR photothermal measurement of substantial heat transport by surface waves of polar amorphous films supported on silicon, *Journal of Applied Physics*, 128 (2020) 095105.
- [34] D.-m. Kim, S. Choi, J. Cho, M. Lim, B.J. Lee, Boosting thermal conductivity by surface plasmon polaritons propagating along a thin Ti film, *Physical Review Letters*, 130 (2023) 176302.

- [35] J. Ordóñez-Miranda, Y.A. Kosevich, B.J. Lee, M. Nomura, S. Volz, Plasmon Thermal Conductance and Thermal Conductivity of Metallic Nanofilms, *Physical Review Applied*, 19 (2023) 044046.
- [36] Z. Pan, G. Lu, X. Li, J.R. McBride, R. Juneja, M. Long, L. Lindsay, J.D. Caldwell, D. Li, Remarkable heat conduction mediated by non-equilibrium phonon polaritons, *Nature*, 623 (2023) 307-312.
- [37] Y. Pei, L. Chen, W. Jeon, Z. Liu, R. Chen, Low-dimensional heat conduction in surface phonon polariton waveguide, *Nature Communications*, 14 (2023) 8242.
- [38] S. Li, J. Wang, Y. Wen, S.J.A.n. Shin, Long Propagating Polaritonic Heat Transfer: Shaping Radiation to Conduction, *ACS Nano*, 18 (2024) 14779–14789.
- [39] H. Casimir, Note on the conduction of heat in crystals, *Physica*, 5 (1938) 495-500.
- [40] J.-P.M. Peraud, N.G. Hadjiconstantinou, Efficient simulation of multidimensional phonon transport using energy-based variance-reduced Monte Carlo formulations, *Physical Review B*, 84 (2011) 205331.
- [41] F. Yang, J. Sambles, G. Bradberry, Long-range surface modes supported by thin films, *Physical Review B*, 44 (1991) 5855-5872.
- [42] I. Dorofeyev, On the equilibrium spectrum of surface polaritons thermally excited by solids, *Physics Letters A*, 375 (2011) 2885-2889.
- [43] J. Burke, G. Stegeman, T. Tamir, Surface-polariton-like waves guided by thin, lossy metal films, *Physical Review B*, 33 (1986) 5186-5201.
- [44] Y. Guo, M. Wang, Heat transport in two-dimensional materials by directly solving the phonon Boltzmann equation under Callaway's dual relaxation model, *Physical Review B*, 96 (2017) 134312.
- [45] Y. Guo, Z. Zhang, M. Nomura, S. Volz, M. Wang, Phonon vortex dynamics in graphene ribbon by solving Boltzmann transport equation with ab initio scattering rates, *International Journal of Heat and Mass Transfer*, 169 (2021) 120981.
- [46] S. Chandrasekhar, *Radiative transfer*, Oxford University Press, Oxford, 1950.
- [47] G.C. Wick, Über ebene Diffusionsprobleme, *Zeitschrift für Physik*, 121 (1943) 702-718.
- [48] S. Gluchko, B. Palpant, S. Volz, R. Braive, T. Antoni, Thermal excitation of broadband and long-range surface waves on SiO₂ submicron films, *Applied Physics Letters*, 110 (2017) 263108.
- [49] P.B. Allen, J.L. Feldman, J. Fabian, F. Wooten, Diffusons, locons and propagons: Character of atomic vibrations in amorphous Si, *Philosophical Magazine B*, 79 (1999) 1715-1731.
- [50] Y. Liao, J. Shiomi, Akhiezer mechanism dominates relaxation of propagons in amorphous material at room temperature, *Journal of Applied Physics*, 130 (2021).
- [51] N. Tambo, Y. Liao, C. Zhou, E.M. Ashley, K. Takahashi, P.F. Nealey, Y. Naito, J. Shiomi, Ultimate suppression of thermal transport in amorphous silicon nitride by phononic nanostructure, *Science Advances*, 6 (2020) eabc0075.
- [52] Z. Zhang, Y. Guo, M. Bescond, J. Chen, M. Nomura, S. Volz, How coherence is governing diffuson heat transfer in amorphous solids, *npj Computational Materials*, 8 (2022) 96.
- [53] M. Krüger, K. Asheichyk, M. Kardar, R. Golestanian, Scale-dependent heat transport in dissipative media via electromagnetic fluctuations, *Physical Review Letters*, 132 (2024) 106903.